Int. J. Electrochem. Sci., 8 **(2013)** 4690 - 4699

International Journal of
ELECTROCHEMICAL
SCIENCE
www.electrochemsci.org

Simulation of Turbulent Flow of a Rotating Cylinder Electrode. Influence of Using Plates and Concentric Cylinder as Counter Electrodes

Tzayam Pérez, José L. Nava[*]

Universidad de Guanajuato, Departamento de Ingeniería Geomática e Hidráulica, Av. Juárez 77, Zona Centro, C.P. 36000, Guanajuato, Guanajuato, México.
[*]E-mail: jlnm@ugto.mx

Received: 4 December 2012 / *Accepted:* 10 February 2013 / *Published:* 1 April 2013

This paper focuses on the effect of plates and a concentric cylinder used as counter electrodes on the turbulent flow of a rotating cylinder electrode (RCE). Four-plate, six-plate, and concentric cylinder counter electrodes were simulated. A 3-D hydrodynamic simulation was performed solving the Reynolds averaged Navier-Stokes (RANS) equation, expressed in terms of turbulent viscosity and the standard turbulence model *k*–ε, with the universal logarithmic wall function boundary conditions. The results of the velocity field 3-D simulations clearly show the formation of turbulent Taylor vortex flow for the four-plate and six-plate arrangements, while in the concentric arrangement, it does not appear. The appearance of Taylor vortex is attributed to the turbulence promoted by the plates. However, this does not imply that the mean velocity profile is favored by the plates; on the contrary, these plates promote the formation of quasi stagnant zones near to them and on the wall of the reactor free of plates. The above findings are important, from the technical and economical standpoints, in the design of this type of electrochemical cell; additionally, such systematic hydrodynamic studies in these cells are rather limited.

Keywords: Rotating cylinder electrode (RCE), Turbulent flow, computational flow dynamics (CFD), Reynolds averaged Navier-Stokes (RANS) equation, Wall functions.

1. INTRODUCTION

The rotating cylinder electrochemical reactor (RCE) is one of the most common geometries for different types of studies, such as metal ion recovery[1-3], alloy formation [1,2], corrosion [1,2], effluent treatment [4-8]and Hull cell studies [9,10].

RCEs are also particularly well suited for high mass transport studies in the turbulent flow regime [2,11-14]. In practical operating conditions, the electrochemical reaction is directly related to

the reactor hydrodynamics [15]. While considering the above, it is important to emphasize that hydrodynamic studies in these cells are rather limited.

The flow pattern in the rotating cylinder cell has been approximated in turbulent flow [16,17]. The theoretical approximation for this pattern has been developed by using the ensemble-averaged Navier-Stokes equation to model turbulent flow around a rotating cylinder, coupling boundary condition of the Dirichlet and Newman [16]. In addition, these authors [16] showed that in the fully turbulent layer, a logarithmic velocity profile exists, which is similar to that developed inside tubes and over flat plates [17]. Another approximation employs the Reynolds Averaged Navier-Stokes (RANS) equations, which include the turbulent viscosity by means of k-ε turbulent model [18,19]. One of the difficulties of using turbulence models is the presence of solid walls, since turbulence models are not applicable in the proximity of the wall [17]. Rivero et al. [18] solved this problem coupling the universal logarithmic wall functions to the rotating and outer boundaries. These authors employed a laboratory scale RCE, with the singularity of the counter electrode in a hexagonal array. The theoretical results showed the presence of Taylor vortices around the cylinder surface [18], which were not observed in the work performed by Hwang and coworkers [16,17].

In previous work carried out by our group, we studied experimentally the influence of using a four-plate, six-plate and concentric cylinder as counter electrodes on mass transport [15].In that research, we found that the counter electrode arrangement has an important role in the hydrodynamic behavior, emphasizing that the four-plate device gives greater turbulence-promoting action on the RCE interface than the others. The above findings are important from a technical and economic standpoint in the design of this type of electrochemical cell. However, theoretical hydrodynamic studies are rather limited.

The objective of the present work is to show the effects of plates and concentric cylinder when used as the counter electrodes on the turbulent flow of a rotating cylinder electrode. Four-plate, six-plate, and concentric cylinder counter electrodes were simulated. A 3-D hydrodynamic simulation was performed by solving a RANS equation, expressed in terms of turbulent viscosity and the standard turbulence model k–ε, with the universal logarithmic wall functions boundary conditions.

2. DESCRIPTION OF THE RCE

Figure 1 shows a schematic diagram of the RCE used as a basis for the computational geometry of each counter electrode arrangement, which were employed to establish the domain of the simulation. The dimensions were taken from Rivera and Nava [15], who used a RCE consisting of 500 cm^3 glass reactor and a 316-type stainless steel cylinder with a 3.8 cm diameter and a length of 11cm, as the cathode. To show the effects of the plates and concentric cylinder devices, a four-plate (Fig. 2(a)), six-plate (Fig. 2(b)), or concentric cylinder was used as the counter electrode (Fig. 2(c)). Each plate used, was a 13 cm long, 2 cm wide and 0.3cm thick RuO_2/TiO_2 DSA. The concentric cylinder, made of the same material, was 11cm long and 7.3 cm in diameter. Table 1 shows the parameters of the RCE cell and the electrolyte properties used by Rivera and Nava [15].

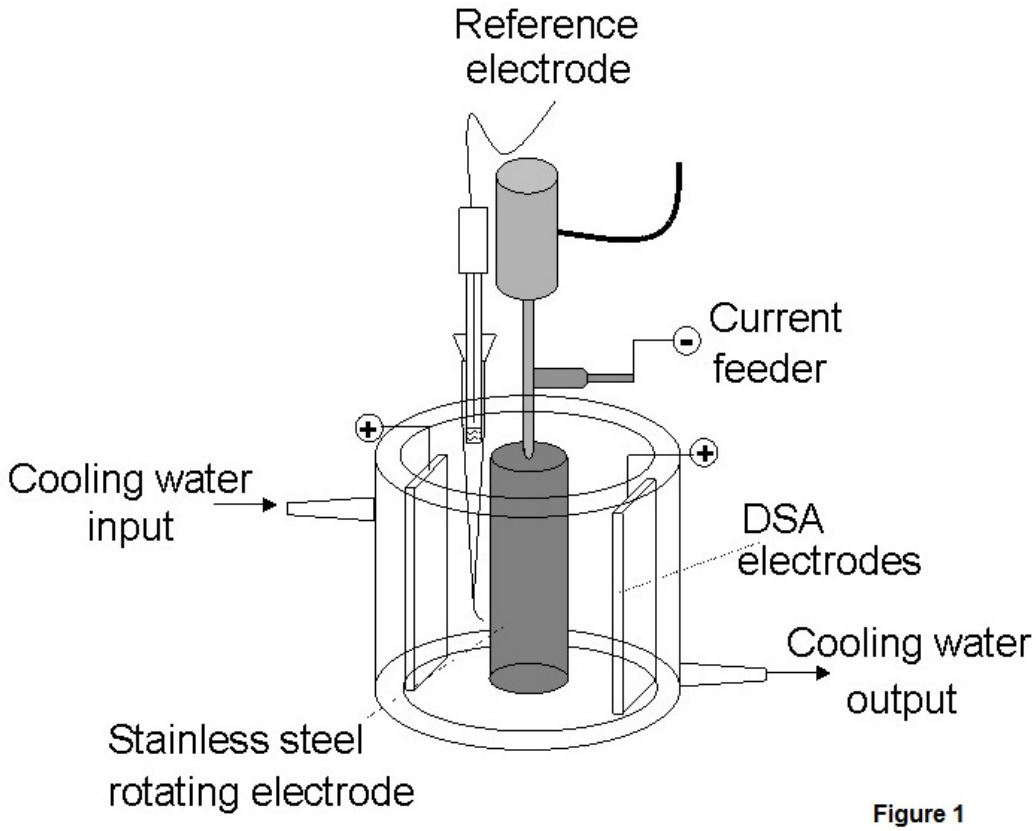

Figure 1. Rotating cylinder electrode scheme.

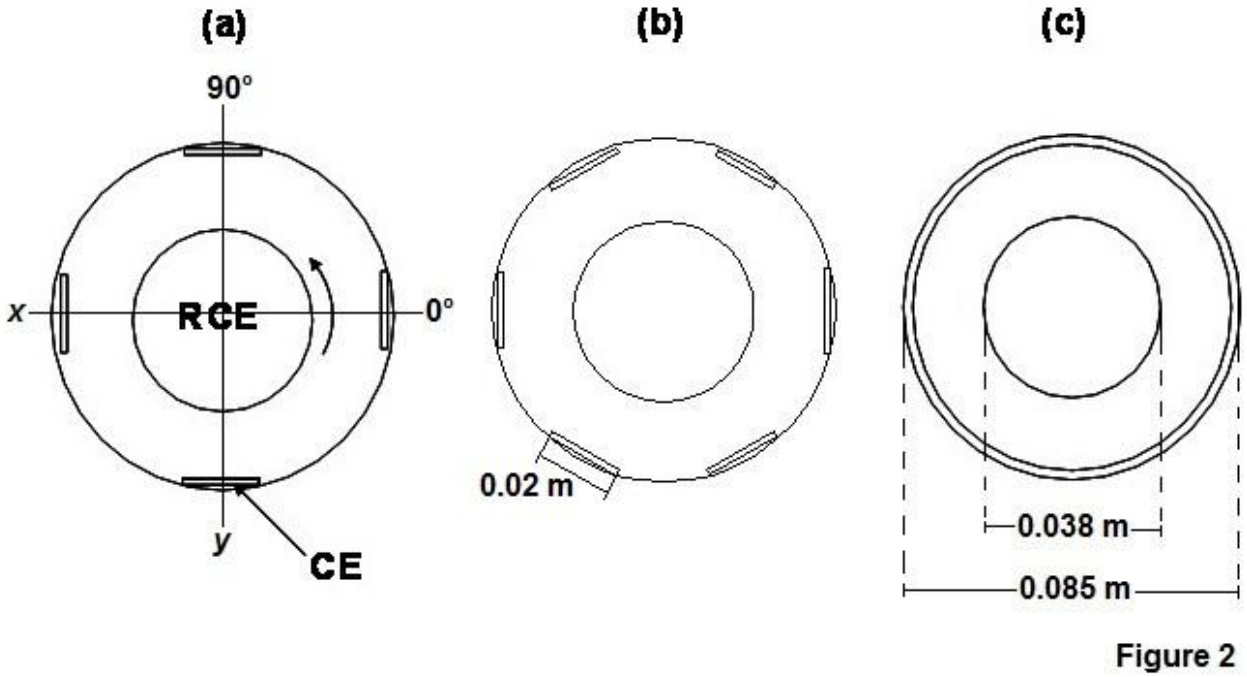

Figure 2. Devices employed as counter electrodes: (a) four-plate, (b) six-plate, and (c) cylinder concentric counter electrodes.

3. FORMULATION OF THE NUMERICAL SIMULATION

For an incompressible fluid under turbulent flow the equations of the model are as follows: Reynolds averaged Navier–Stokes (1), where the so-called Reynolds stresses are expressed in terms of turbulent viscosity and the standard turbulence model k–ε (Eq.(2)):

$$(\boldsymbol{\rho u \nabla})\boldsymbol{u} = -\nabla P + \nabla\left(\mu + \mu_T\right)(\nabla \boldsymbol{u} + \nabla \boldsymbol{u}^T) + \boldsymbol{F} \qquad (1)$$

$$\mu_T = \rho C_\mu \frac{k^2}{\varepsilon} \qquad (2)$$

where u is the average velocity vector, P the pressure, μ the viscosity, μ_T the turbulent viscosity, F the external force, ρ the density, C_μ is a turbulence model constant, k is the turbulent kinetic energy and ε the turbulent energy dissipation rate.

Table 1. RCE reactor parameters and electrolyte properties [15].

Reaction Volume, V_R	350 cm^3
Reactor diameter,	8.5 cm
RCE diameter, d	3.8 cm
RCE length	11 cm
RCE area, A_{RCE} (in contact with electrolyte)	80 cm^2
Length and width of the plates used as anodes (attached to the reactor walls)	13 cm × 2 cm
Length of the concentric counter electrode (attached to the reactor walls)	11 cm
Concentric counter electrode diameter	7.3 cm
Anode and cathode gap	1.75 cm
Counter electrode area, A_{CE}, (four plates, in contact with the solution)	56 cm^2
Counter electrode area, A_{CE}, (six plates, in contact with the solution)	84 cm^2
Counter electrode area, A_{CE}, (concentric, in contact with the solution)	153.7 cm^2
Kinematic Viscosity, ν	0.01 $cm^2\ s^{-1}$

This model is applicable at high Reynolds numbers; for this reason, the near-wall regions, where the velocity is relative to the wall, these decrease quickly and are inaccessible in this model. To solve this problem, wall functions are usually used. These functions are based on a universal velocity distribution, which in a turbulent layer is described with the following equation (3) [16-18,20]:

$$u^+ = 2.5 ln y^+ + 5.5 \qquad (3)$$

were u^+ is the normalized velocity component, and y^+ is the dimensionless distance from the wall.

The corresponding boundary conditions are as follows:

- Shear stress, $\tau = 0$ at the fluid surface.
- Velocity u^+ given by equation (3) at a distance y^+ from solid surface, for all other boundaries, where u^+ corresponds to the dimensionless velocity with respect to solid surface.

After verifying the solution at different values of y^+ and step sizes, the value of y^+ was fixed at 60. This value is in the fully turbulent region ($20 < y^+ < 400$), where the turbulent stresses and fluxes are more important [16].

Equations (1), (2) and (3) were solved numerically in 3-D through finite elements by using commercial software COMSOL Multiphysics (4.3). A simulation domain for concentric, 4 plates, and 6 plates with 50108, 58237, and 52615 tetrahedral mesh elements was respectively considered. Using a computer with two Intel®Xeon™ 2.30 GHz processors, 96 GB of RAM, and 64 bits of operative system, the typical solution around these mesh elements did not change. The simulation run times were about 40 to 60 min depending on the geometry of the reactor; 6 plates required more run times. RCE reactor parameters and electrolyte properties are shown in Table 1.

4. RESULTS AND DISCUSSION

Figure 3(a) shows the velocity field for the domain of the simulation, calculated at 900 rpm for a four-plate counter electrode. Figure 3(b) shows a surface plot of the velocity field in two cases: in front of the plate used as counter electrode and in front of the reactor wall, in the area which is free of an anode plate. From the analysis of the simulation, the turbulent Taylor vortex flow was shown to form three high velocity zones, which can be observed along to the *z* coordinate at 0.012, 0.039 and 0.067 m, respectively, close to the rotating cylinder surface. Moreover, it is important to note the appearance of low velocity regions (quasi stagnant zones), close to the counter electrode plates and on the wall of the reactor, free of anode plates, which are developed by the static boundaries. From the analysis of this figure, it can be clearly observed that the quasi stagnant zones accumulate more on the wall than on the plate used as counter electrode. The presence of turbulent Taylor vortex flow was reported by Rivero et al. [18].

Figures 4 (a) and (b) show the velocity profiles in radial direction, in front of the plates, calculated at 900 rpm for a four-plate counter electrode at two heights, 0.025 and 0.039 m, corresponding respectively to the quasi stagnant and high velocity zones. In proximity of the rotating electrode, Figure 4 (a), the velocity decreases exponentially, from 0.455 to 0.183 m s^{-1} between $0.019 \leq r \leq 0.023$ m, while the velocity profile remains almost constant (0.17 m s^{-1}) between $0.023 \leq r \leq 0.031$ m, similar to the Prandl layer which is typically developed in the annular concentric cylinder [11]. Finally, the velocity decreases linearly from 0.145 to 0.048 m s^{-1} when $r \geq 0.031$ m. On the other hand, the high velocity profile (Figure 4(b)) does not present different velocity zones and this velocity decays hyperbolically from 0.59 to 0.08 m s^{-1} between $0.019 \leq r \leq 0.0425$ m.

Figures 5 (a) and (b) show the velocity profiles in radial direction, for the walls free of plate, calculated at 900 rpm for a four-plate counter electrode at two heights, 0.025 and 0.039 m, corresponding respectively to the quasi stagnant and high velocity zones [18,19]. The quasi stagnant

profile (Figure 5(a)) decreases exponentially from 0.45 to 0.15 m s^{-1} between $0.019 \leq r \leq 0.023$ m, and then between $0.023 \leq r \leq 0.0425$ m, the velocity decreases gradually from 0.15 to 0 m s^{-1}.

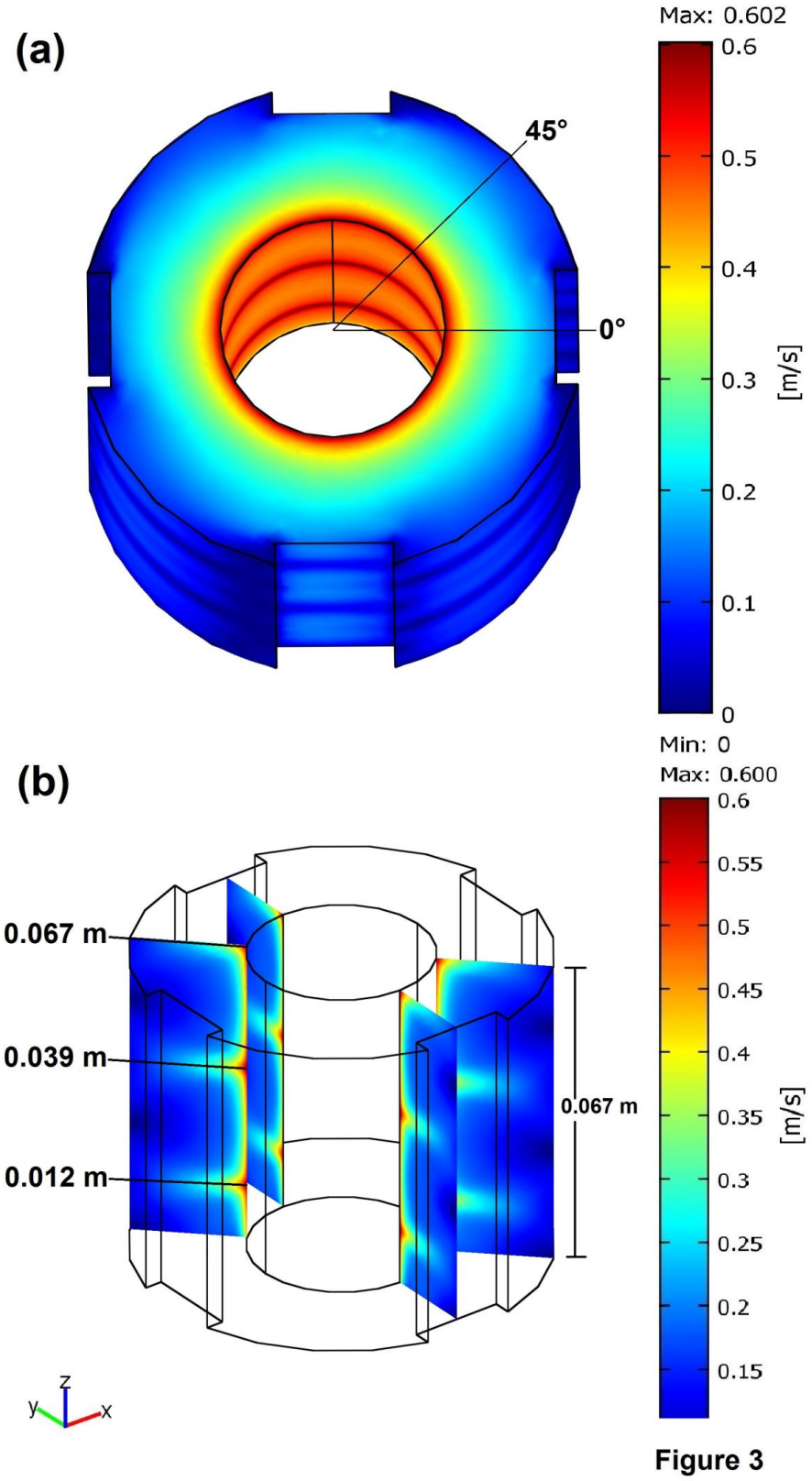

Figure 3. Simulation of the hydrodynamics of a RCE with four-plate counter electrodes at 900 rpm: (a) velocity field; (b) surface plot of the velocity field.

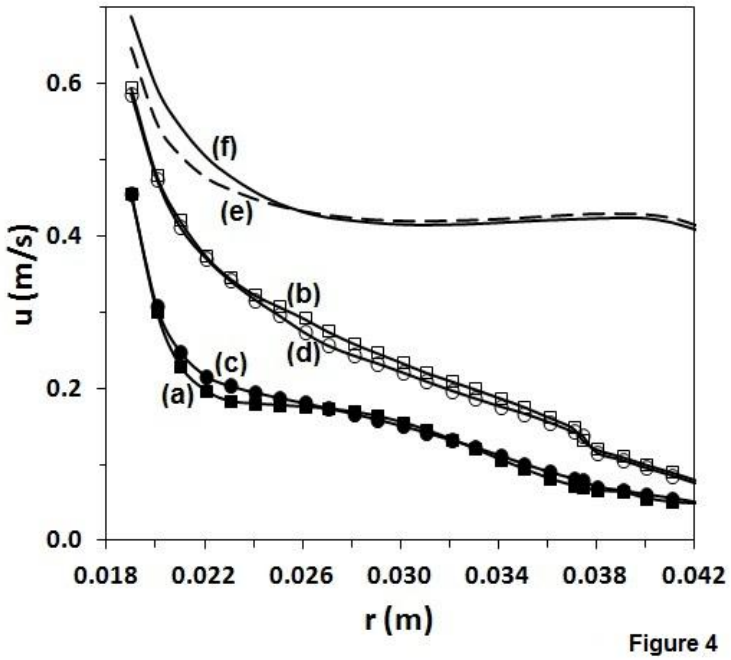

Figure 4. Profile of the velocity field in radial direction, in front the plates: four-plates at (a) z = 0.025 m, 0^o; and at (b) z = 0.039 m, 0^o.Six-plates at (c) z = 0.020 m, 0^o; and at (d) z = 0.032 m, 0^o. The profile calculated in concentric cylinder: (e) z = 0.022 m,0^o; and at (f) z = 0.014 m, 0^o.

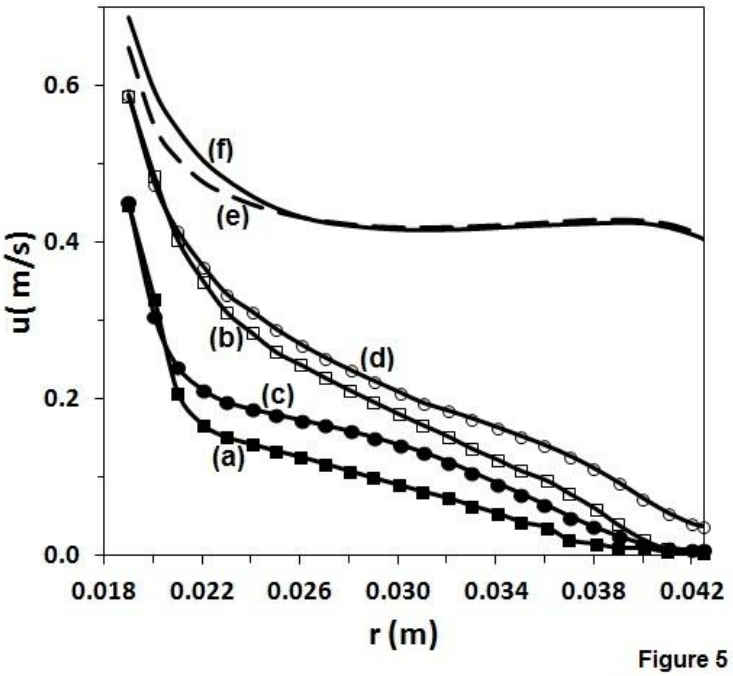

Figure 5. Profile of the velocity field, in radial direction in front of the walls free of anode plates. Device: four-plates at (a) z = 0.025 m, 45^o; and (b) z = 0.039 m, 45^o. Six-plates at (c) z = 0.020 m, 30^o; and (d) z = 0.032 m, 30^o. The profile calculated in the concentric cylinder: (e) z = 0.022 m, 0^o; and (f) z = 0.014 m, 0^o.

The high velocity profile (Figure 5 (b)) decreases hyperbolically from 0.59 to 0.0 m s^{-1}, between $0.019 \leq r \leq 0.0425$ m, which is similar to the results shown in Figure 4 (b).

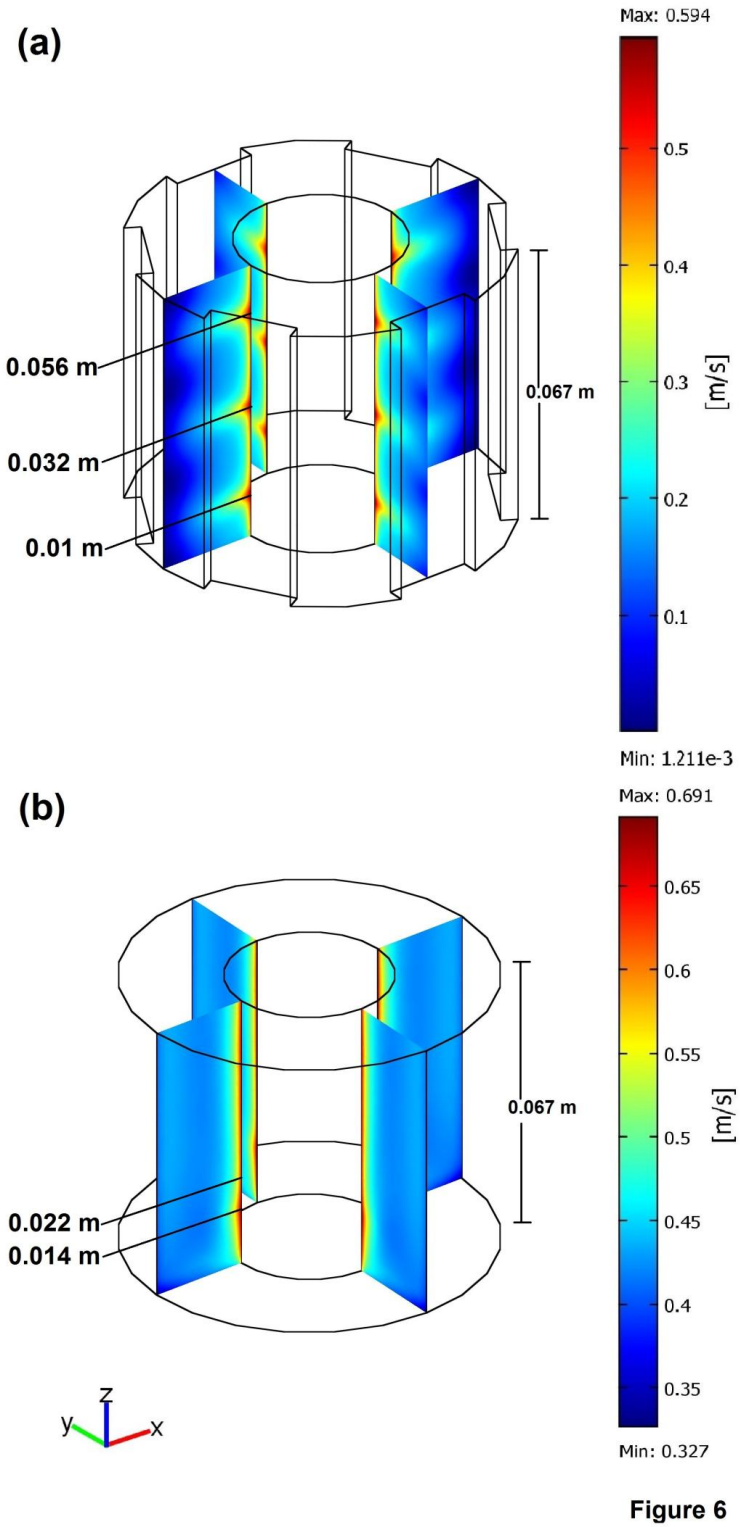

Figure 6. Surface plot of the velocity field of a RCE at 900rpm with: (a) six-plate, (b) concentric counter electrodes.

Figures 6 (a) and (b) show a surface plot of the velocity field for a six-plate and a concentric counter electrode, respectively, at 900 rpm. The velocity field developed in Figure 6(a) is similar to that obtained with a four-plate arrangement (Figure 3 (b)), the turbulent Taylor vortex flow forming

three high velocity zones along to the z coordinate at 0.01, 0.032 and 0.056 m. Figure 6 (a) also presents quasi stagnant zones close to the plate used as a counter electrode and on the plate-free wall of the reactor. On the contrary, the velocity field developed for the concentric counter electrode device (Figure 6 (b)) did not develop Taylor vortex flow; therefore the velocity field did not show quasi stagnant regions, except for a very small region close to the outer wall on the bottom of the reactor. It is important to note that only one moderate high velocity zone at 0.014 m appears on the rotating electrode (Figure 6(b)). Comparing Figure 3 (b) with Figures 6 (a) and (b) confirms the influence of the counter electrode arrangement on the hydrodynamics of the RCE. This last is in agreement to that obtained by Rivero in [18].

Figures 4(c) and (d) show the velocity profiles for six-plate device, developed in front of the plate, at two heights 0.020 and 0.032 m, corresponding respectively to the quasi stagnant and high velocity zones [18,19]. It can be clearly observed that the above profiles have a very close behavioral pattern to those presented in the four-plate device. Conversely, for the concentric device, Figures 4(e) and (f), the velocity profiles are higher relative to those developed in the four-plate and six-plate devices. The profiles depicted in Figure 4(e) at height of 0.022 m corresponds to the moderate velocity, which decreases exponentially from 0.65 to 0.4 m s^{-1}; while the velocity profile at height of 0.014 m, corresponding to the high velocity profile, also decreases exponentially from 0.69 to 0.4 m s^{-1}.

Figures 5(c) and (d) show the velocity profiles for the plate-free walls at 0.20 and 0.032 m, corresponding respectively to the low and high velocity zones. The velocity in Figure 5(c) decreases hyperbolically from 0.45 to 0.007 m s^{-1}between $0.019 \leq r \leq 0.0425$ m; and the velocity in Figure 5(d) also decrease hyperbolically, from 0.59 to 0.037 m s^{-1}, between $0.019 \leq r \leq 0.0425$ m.

The hydrodynamics in the six-plate device, Figures 4 (c) and (d), and Figures 5 (c) and (d), present higher velocities than those found for the corresponding four-plate device, Figures 4 (a) and (b), and Figures 5 (a) and (b). Nevertheless, these velocities were lower than those obtained for the concentric arrangement, Figures 4 (e) and (f), and Figures 5 (e) and (f).

The hydrodynamics for the concentric arrangement was superior relative to four-plate and six-plate counter electrodes, since plates promote quasi stagnant zones in their proximity and on the plate-free wall [18].

5. CONCLUSIONS

This investigation shows the effect of a four-plate, six-plate and concentric cylinder counter electrodes on the turbulent flow of a rotating cylinder electrode. A 3-D hydrodynamic simulation performed by solving a RANS equation, expressed in terms of turbulent viscosity and the standard turbulence model k–ε, with the universal logarithmic wall functions boundary conditions.

Results of 3-D simulations of the velocity field show clearly the formation of the turbulent Taylor vortex flow for the four-plate and six-plate counter electrodes, while in the concentric this is not present. The appearance of the Taylor vortex is attributed to the turbulence promoted by the plates. However, it does not imply that the mean velocity field is not increased by the plates.

The maximum velocity on the rotating surface, for the device equipped with six-plate counter electrodes, gave a value of 0.59 m s^{-1}, which is similar to that obtained from the four-plate arrangement; while the velocity for the concentric counter electrode was 0.69 m s^{-1}.

On the other hand, the maximum velocities developed on the plate surface were 0.08 and 0.075 m s^{-1}, for the devices employing the four-plate and six-plate counter electrodes; while the maximum velocities were 0.005 and 0.037 m s^{-1}, on the plate-free wall surface for the four-plate and six-plate arrangements, respectively. These values were lower than that obtained on the concentric surface, which was 0.4 m s^{-1}.

The hydrodynamics of the concentric was superior to those of the four-plate and six-plate counter electrodes, since plates develop quasi stagnant zones in their proximity and on the plate-free wall of the reactor.

ACKNOWLEDGEMENTS
T. Pérez is grateful to CONACYT for the scholarship No. 366128 granted. The authors thank Gretchen T. Lapidus Lavine for her help in the manuscript revision. The authors are grateful to CONACYT for the economic support via the project No. 118872.

References

1. D. R. Gabe, G. D. Wilcox, J. Gonzalez-Garcia and F. C. Walsh, *J. Appl. Electrochem.*, 28 (1998) 759.
2. J. Low, C. Ponce de León and F. C. Walsh, *Aust. J. Chem.*, 58 (2005) 246.
3. J. L. Nava, E. Sosa, C. Ponce de León and M.T. Oropeza, *Chem. Eng. Sci.*, 56 (2001) 2695.
4. G. Chen, *Sep. Purif. Technol.*, 38 (2004) 11.
5. J. M. Grau and J. M. Bisang, *J. Chem. Technol. Biot.*, 77 (2002) 465.
6. F. F. Rivera, I. González and J. L. Nava, *Environ. Technol.*, 29 (2008) 817.
7. F. C. Walsh, *The role of the rotating cylinder electrode*, in: J. D. Genders, N. L. Weinberg(Eds.),*Electrochemistry for a Cleaner Environment*, The Electrosynthesis company, New York (1992).
8. F. C. Walsh, *Pure Appl. Chem.*, 73 (2001) 1819.
9. C. Madore, M. Matlosz and D. Landolt, *J. Appl. Electrochem.*, 22 (1992) 1155.
10. N. Zech, E. J. Podlaha and D. Landolt, *J. Appl. Electrochem.*, 28 (1998) 1251.
11. D. R. Gabe, *J. Appl. Electrochem.*, 4 (1974) 91.
12. D. R. Gabe and F. C. Walsh, *J. Appl. Electrochem.*, 14 (1984) 555.
13. J. M. Grau and J. M. Bisang, *J.Appl.Electrochem.*, 36 (2006) 759.
14. A. H. Nahlé, G. W. Reade and F. C. Walsh, *J. Appl. Electrochem.*, 25 (1995) 450.
15. F. F. Rivera and J. L. Nava, *Electrochim. Acta*, 52 (2007) 5868.
16. J. Y. Hwang, K. S. Yang and K. Bremhorst, *J. Fluid Eng.*, 129 (2007) 40.
17. J. Y. Hwang, K. S. Yang, D. H. Yoon and K. Bremhorst, *Int. J. Heat Fluid Fl.*, 29 (2008) 1268.
18. E. P. Rivero, P. Granados, F. F. Rivera, M. Cruz and I. González, *Chem. Eng. Sci.*, 65 (2010) 3042.
19. J. A. Delgadillo, R. Enciso, C. Ojeda, I. Rodríguez, *Int. J. Electrochem. Sci.*, 7 (2012) 2065.
20. P. S. Bernard and J. M. Wallace, Turbulent flow: Analysis, Measurement, and Prediction, John Wiley & Sons, New Jersey(2002)